Scattering and Radiation from a Slitted Parallel-Plate with Rectangular Grooves: TE-Wave

Jung Hyeong Lee and Hyo Joon Eom, *Member, IEEE*

***Abstract*— TE-wave scattering and radiation from a slitted parallel-plate waveguide with rectangular grooves is considered. The Fourier transform and the mode matching are used to represent the scattered field in terms of the continuous and discrete modes. The simultaneous equations for the discrete modal coefficients are obtained by matching the boundary conditions. The fast-converging series solutions are presented to evaluate the far-zone radiation, reflection, and transmission coefficients. The numerical computations illustrate the angular behaviors of far-zone radiation in terms of the slit size, groove size, and operating frequency. The antenna radiation pattern of the slitted parallel-plate is measured and compared with the theory.**

***Index Terms*—Electromagnetic radiation, electromagnetic scattering.**

I. Introduction

ELECTROMAGNETIC scattering from a slitted parallel-plate waveguide is an important subject matter for its leaky-wave antenna applications [1]–[4]. Recently, we have investigated the radiation from finite thick slits in a parallel-plate waveguide by utilizing the Fourier transform and the mode matching [5]. In this paper, we investigate TE-wave (transverse electric to wave propagation) radiation from a slitted parallel-plate waveguide with rectangular grooves. The purpose of the present paper is, in particular, to study the effect of the rectangular grooves on the antenna radiation pattern. An analytical method to solve the scattering problem is the Fourier transform and the mode-matching technique as used in [5]. Using the residue calculus, we represent the transmission, reflection, and scattering coefficients in fast-convergent series forms which are computationally very efficient. In the next two sections, we present the scattered fields for the TE-wave and perform the numerical computations for transmission, reflection, and scattering. A brief summary of the scattering analysis is given in the conclusion. The notations in this paper closely follow those in [5].

II. Field Representations

Consider TE-wave scattering from N_s slits (width $2a_s$, thickness t, interval T_s) and N_g grooves (width $2a_g$, depth d, interval T_g) in a parallel-plate waveguide shown in Fig. 1. Regions (I)–(IV), respectively, denote N_g grooves (wavenumber $= k_1 = \omega\sqrt{\mu_0\epsilon_1}$), the parallel-plate waveguide (wavenumber $= k_2 = \omega\sqrt{\mu_0\epsilon_2}$), N_s slits (wavenumber $= k_3 = \omega\sqrt{\mu_0\epsilon_3}$), and the upper half-space (wavenumber $= k_4 = \omega\sqrt{\mu_0\epsilon_4} = 2\pi/\lambda$). Assume two incident waves E_y^{i1} and E_y^{i2} propagating in Regions (II) and (IV), respectively. A time-harmonic factor $e^{-i\omega t}$ is suppressed. In Region (I) the total field is

$$E_y^{\mathrm{I}}(x,z) = \sum_{m=1}^{\infty} u_m^l \sin a_{gm}(x - x_d + a_g - lT_g)\sin\xi_m(z+d) \tag{1}$$

where $a_{gm} = m\pi/2a_g$, $\xi_m = \sqrt{k_1^2 - a_{gm}^2}$, $l = -L_1^g, \cdots, L_2^g$, and $N_g = L_1^g + L_2^g + 1$.

In Region (II), the total field consists of the incident and scattered fields as

$$E_y^{i1}(x,z) = A_1 e^{ik_{xs}x}\sin(k_{zs}z) \tag{2}$$

$$E_y^{\mathrm{II}}(x,z) = \frac{1}{2\pi}\int_{-\infty}^{\infty}[\tilde{E}_{\mathrm{II}}^{+}(\zeta)e^{i\kappa_2 z} + \tilde{E}_{\mathrm{II}}^{-}(\zeta)e^{-i\kappa_2 z}]e^{-i\zeta x}\,d\zeta \tag{3}$$

where $0 < s < k_2 h/\pi$ (s: integer), $k_{zs} = s\pi/h$, $k_{xs} = \sqrt{k_2^2 - k_{zs}^2}$, and $\kappa_2 = \sqrt{k_2^2 - \zeta^2}$. The Fourier transform of $E_y^{\mathrm{II}}(x,0)$ is defined as $\int_{-\infty}^{\infty} E_y^{\mathrm{II}}(x,0)e^{i\zeta x}\,dx$, which is given by $[\tilde{E}_{\mathrm{II}}^{+}(\zeta) + \tilde{E}_{\mathrm{II}}^{-}(\zeta)]$.

In Region (III) ($wT_s - a_s < x < wT_s + a_s$, $h < z < h + t$: $w = -L_1^s, \cdots, L_2^s$, $N_s = L_1^s + L_2^s + 1$), the total transmitted field is

$$E_y^{\mathrm{III}}(x,z) = \sum_{k=1}^{\infty}\sin a_{sk}(x + a_s - wT_s) \times [b_k^w \cos\chi_k(z-h) + c_k^w \sin\chi_k(z-h)] \tag{4}$$

where $a_{sk} = k\pi/(2a_s)$ and $\chi_k = \sqrt{k_3^2 - a_{sk}^2}$.

In Region (IV), the total field is

$$E_y^{i2}(x,z) = A_2 e^{i[-k_x x - k_z(z-h-t)]} \tag{5}$$

$$E_y^{r}(x,z) = -A_2 e^{i[-k_x x + k_z(z-h-t)]} \tag{6}$$

$$E_y^{s}(x,z) = \frac{1}{2\pi}\int_{-\infty}^{\infty}\tilde{E}_y^s(\zeta)e^{-i\zeta x + i\kappa_4(z-h-t)}\,d\zeta \tag{7}$$

where $\kappa_4 = \sqrt{k_4^2 - \zeta^2}$, $k_x = k_4\sin\theta$, and $k_z = k_4\cos\theta$.

To determine unknown coefficients c_m^w, b_m^w, and u_m^l, it is necessary to enforce the boundary conditions of the field continuities. Utilizing the Fourier transform technique as used to obtain (8) in [5], the tangential electric field continuity at

Manuscript received October 22, 1997; revised July 2, 1998. This work was supported by the Institute of Information Technology Assessment, Korea, Contract 96147-RT-12.

The authors are with the Department of Electrical Engineering, Korea Advanced Institute of Science and Technology, Yusung Gu, Taejon, Korea.

Publisher Item Identifier S 0018-926X(98)07491-2.

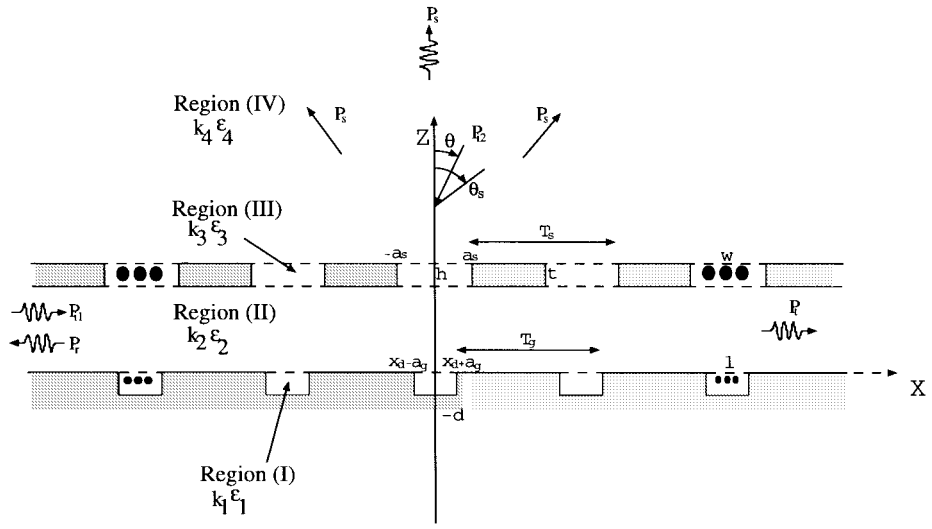

Fig. 1. Problem geometry—slitted parallel-plate with rectangular grooves.

$z = 0$ yields

$$\tilde{E}_{\rm II}^{+}(\zeta) + \tilde{E}_{\rm II}^{-}(\zeta) = \sum_{l=-L_1^g}^{L_2^g} \sum_{m=1}^{\infty} u_m^l a_{gm} a_g^2 \sin(\xi_m d) \times F_m(a_g\zeta) e^{i\zeta(x_d + lT_g)} \quad (8)$$

$$F_m(t) = \frac{e^{it}(-1)^m - e^{-it}}{t^2 - (m\pi/2)^2}. \quad (9)$$

The tangential electric field continuity at $z = h$ yields

$$\tilde{E}_{\rm II}^{+}(\zeta) e^{i\kappa_2 h} + \tilde{E}_{\rm II}^{-}(\zeta) e^{-i\kappa_2 h} = \sum_{w=-L_1^s}^{L_2^s} \sum_{k=1}^{\infty} b_k^w a_{sk} a_s^2 F_k(a_s\zeta) e^{i\zeta w T_s}. \quad (10)$$

The tangential electric field continuity at $z = h + t$ yields

$$\tilde{E}_y^s(\zeta) = \sum_{w=-L_1^s}^{L_2^s} \sum_{k=1}^{\infty} [b_k^w \cos \chi_k t + c_k^w \sin \chi_k t] \times a_{sk} a_s^2 F_k(a_s\zeta) e^{i\zeta w T_s}. \quad (11)$$

We multiply the tangential magnetic field continuity ($H_x^{i1} + H_x^{\rm II} = H_x^{\rm I}$) on the aperture of the grooves ($lT_g + x_d - a_g < x < lT_g + x_d + a_g$, $z = 0$: $l = -L_1^g, \cdots, L_2^g$) by $\sin a_{gn}(x - x_d + a_g - rT_g)$. Then we integrate it with respect to x from $rT_g + x_d - a_g$ to $rT_g + x_d + a_g$ to obtain

$$\begin{aligned} &\sum_{w=-L_1^s}^{L_2^s} \sum_{k=1}^{\infty} a_{sk} a_{gn} a_s^2 a_g^2 \times \frac{1}{2\pi} I_{nk}^{rw}(a_g, a_s, -x_d - rT_g + wT_s) b_k^w \\ &- \sum_{l=-L_1^g}^{L_2^g} \sum_{m=1}^{\infty} a_{gm} a_{gn} a_g^4 \times \sin(\xi_m d) \frac{1}{2\pi} J_{nm}^{rl}(a_g, (l-r)T_g) u_m^l \\ &- a_g \xi_m \cos(\xi_m d) \delta_{nm} \delta_{rl} u_m^l \\ &= -A_1 k_{zs} a_{gn} a_g^2 F_n(a_g k_{xs}) e^{ik_{xs}(x_d + rT_g)} \end{aligned} \quad (12)$$

where $I_{nk}^{rl}(\alpha, \beta, \gamma)$ is an integral representing a mode coupling between the groove and the slit. Similarly, $J_{nm}^{rl}(\alpha, \gamma)$ represents a coupling mechanism between the grooves (or slits) through Region (II). Fig. 2 shows a graphical interpretation of the integrals $I_{nk}^{rl}(\alpha, \beta, \gamma)$ and $J_{nm}^{rl}(\alpha, \gamma)$. It is expedient to transform the integrals into rapidly converging series by utilizing the residue calculus as

$$I_{nk}^{rl}(\alpha, \beta, \gamma) = \int_{-\infty}^{\infty} \frac{\kappa_2}{\sin \kappa_2 h} F_n(-\alpha\zeta) F_k(\beta\zeta) e^{-i\zeta\gamma} \, d\zeta \quad (13)$$

$$\begin{aligned} &= \frac{1}{\alpha^2\beta^2} [(-1)^{n+k} I(\alpha, \beta, \alpha - \beta + \gamma) \\ &\quad - (-1)^n I(\alpha, \beta, \alpha + \beta + \gamma) \\ &\quad - (-1)^k I(\alpha, \beta, -\alpha - \beta + \gamma) \\ &\quad + I(\alpha, \beta, -\alpha + \beta + \gamma)] \end{aligned} \quad (14)$$

$$I(\alpha, \beta, q) = \int_{-\infty}^{\infty} \frac{\kappa_2}{\sin \kappa_2 h} \frac{e^{-iq\zeta}}{(\zeta^2 - \alpha_n^2)(\zeta^2 - \beta_k^2)} \, d\zeta \quad (15)$$

$$= \begin{cases} A & \text{if } \alpha_n \neq \beta_k \\ B & \text{if } \alpha_n = \beta_k \end{cases} \quad (16)$$

where as shown in (17)–(19), at the bottom of the next page, and $\alpha_n = n\pi/(2\alpha)$, $\beta_k = k\pi/(2\beta)$, $\eta_1 = \sqrt{k_2^2 - \alpha_n^2}$, $\eta_2 = \sqrt{k_2^2 - \beta_k^2}$. Note that (19) is similar to (11) in [6].

From the tangential magnetic field continuity on the aperture of the slits ($wT_s - a_s < x < wT_s + a_s$, $z = h$: $w = -L_1^s, \cdots, L_2^s$) and the orthogonality of $\sin a_{sp}(x + a_s - vT_s)$, we obtain

$$\begin{aligned} &\sum_{w=-L_1^s}^{L_2^s} \sum_{k=1}^{\infty} a_{sk} a_{sp} a_s^4 \times \frac{1}{2\pi} J_{pk}^{vw}[a_s, (w-v)T_s] b_k^w - \chi_k a_s \delta_{pk} \delta_{vw} c_k^w \\ &- \sum_{l=-L_1^g}^{L_2^g} \sum_{m=1}^{\infty} a_{sp} a_{gm} a_s^2 a_g^2 \times \sin(\xi_m d) \frac{1}{2\pi} I_{pm}^{vl}(a_s, a_g, x_d + lT_g - vT_s) u_m^l \\ &= -A_1 k_{zs} a_{sp} a_s^2 \cos(k_{zs} h) F_p(a_s k_{xs}) e^{ik_{xs} vT_s}. \end{aligned} \quad (20)$$

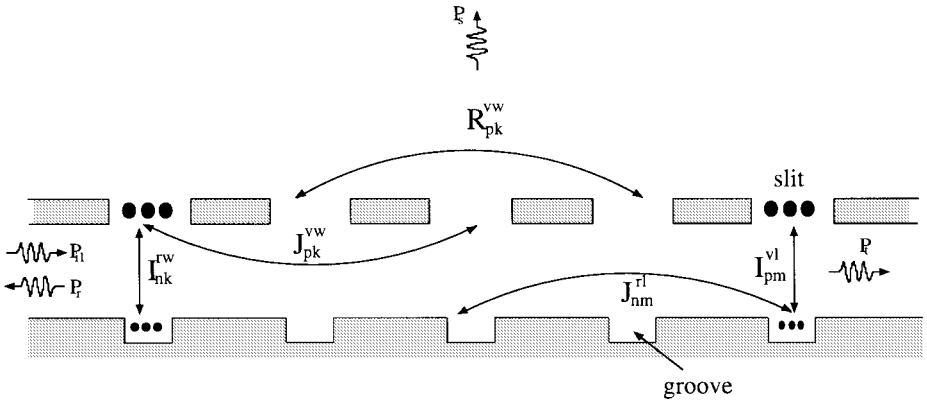

Fig. 2. Coupling phenomena between grooves and slits.

From the tangential magnetic field continuity on the aperture of the slits ($wT_s - a_s < x < wT_s + a_s$, $z = h + t$: $w = -L_1^s, \cdots, L_2^s$) and the orthogonality of $\sin a_{sp}(x + a_s - vT_s)$, we obtain

$$\sum_{w=-L_1^s}^{L_2^s} \sum_{k=1}^{\infty} \left[a_{sk} a_{sp} a_s^4 \cos(\chi_k t) \frac{i}{2\pi} R_{pk}^{vw} + a_s \chi_k \sin(\chi_k t) \delta_{pk} \delta_{vw} \right] b_k^w + \sum_{w=-L_1^s}^{L_2^s} \sum_{k=1}^{\infty} \left[a_{sk} a_{sp} a_s^4 \sin(\chi_k t) \frac{i}{2\pi} R_{pk}^{vw} - a_s \chi_k \cos(\chi_k t) \delta_{pk} \delta_{vw} \right] c_k^w = 2iA_2 k_z a_{sp} a_s^2 F_p(-a_s k_x) e^{-ik_x v T_s} \tag{21}$$

where

$$R_{pk}^{vw} = \int_{-\infty}^{\infty} \kappa_4 F_p(-a_s\zeta) F_k(a_s\zeta) e^{i\zeta(w-v)T_s} \, d\zeta \tag{22}$$

$$= \frac{2\pi\sqrt{k_4^2 - a_{sp}^2}}{a_s^3 a_{sp}^2} \delta_{pk}\delta_{wv} - r_{pk}^{vw} \tag{23}$$

$$r_{pk}^{vw} = \frac{2}{a_s^4} \{[(-1)^{p+k} + 1] I_3(qT_s) - (-1)^k I_3(qT_s + 2a) - (-1)^p I_3(qT_s - 2a)\} \tag{24}$$

$$q = w - v \tag{25}$$

$$I_3(c) = \int_0^{\infty} \frac{i\sqrt{v(v-2i)} e^{ik_4|c|} e^{-k_4|c|v}}{k_4^2 \left[(1+iv)^2 - \frac{a_{sp}^2}{k_4^2} \right] \left[(1+iv)^2 - \frac{a_{sk}^2}{k_4^2} \right]} \, dv. \tag{26}$$

The R_{pk}^{vw} represents an interaction between the slits through Region (IV). The expressions similar to R_{pk}^{vw} are given in [5]. It is possible to solve the simultaneous systems (12), (20), and (21) for b_k^w, c_k^w, and u_m^l

III. Evaluation of Scattered Fields

By use of the residue calculus, we evaluate the total scattered fields at $x = \pm\infty$

$$E_y^{\mathrm{II}}(\pm\infty, z) = \sum_{v=1}^{\infty} (-1)^v K_v(\mp k_{xv}) \sin(k_{zv} z) e^{\pm ik_{xv} x} \tag{27}$$

where $0 < v < k_2 h/\pi$, v: integer, $k_{zv} = v\pi/h$, $k_{xv} = \sqrt{k_2^2 - k_{zv}^2}$ and

$$K_v(\zeta) = \frac{ik_{zv}[\alpha_1(\zeta) - (-1)^v \alpha_2(\zeta)]}{-k_{xv} h} \tag{28}$$

$$\alpha_1(\zeta) = \sum_{w=-L_1^s}^{L_2^s} \sum_{k=1}^{\infty} b_k^w a_{sk} a_s^2 F_k(a_s\zeta) e^{i\zeta w T_s} \tag{29}$$

$$A = \frac{-\pi\eta_1 \sin(|q|\alpha_n)}{\alpha_n(\alpha_n^2 - \beta_k^2)\sin(\eta_1 h)} + \frac{\pi\eta_2 \sin(|q|\beta_k)}{\beta_k(\alpha_n^2 - \beta_k^2)\sin(\eta_2 h)} - 2\pi i \sum_{v=1}^{\infty} (-1)^v \frac{\kappa_2^2 e^{i|q|\zeta}}{\zeta h(\zeta^2 - \alpha_n^2)(\zeta^2 - \beta_k^2)} \Bigg|_{\zeta=\zeta_v} \tag{17}$$

$$B = \frac{-\pi}{2\alpha^3 (\sin\eta_1 h)^2} \left\{ \alpha_n \sin\eta_1 h [|q|\eta_1 \cos(|q|\alpha_n) - \frac{\alpha_n}{\eta_1} \sin(|q|\alpha_n)] + \sin(|q|\alpha_n)[\alpha_n^2 h \cos\eta_1 h - \eta_1 \sin\eta_1 h] \right\} - 2\pi i \sum_{v=1}^{\infty} (-1)^v \frac{\kappa_2^2 e^{i|q|\zeta}}{\zeta h(\zeta^2 - \alpha_n^2)(\zeta^2 - \beta_k^2)} \Bigg|_{\zeta=\sqrt{k_2^2 - (v\pi/h)^2}} \tag{18}$$

$$J_{nm}^{rl}(\alpha, \gamma) = \int_{-\infty}^{\infty} \frac{\kappa_2}{\tan\kappa_2 h} F_n(-\alpha\zeta) F_m(\alpha\zeta) e^{i\zeta\gamma} \, d\zeta = \frac{2\pi\eta_n \cot(\eta_n h)}{\alpha^3 \alpha_n^2} \delta_{nm}\delta_{rl} + j_{nm}^{rl} \tag{19}$$

$$j_{nm}^{rl} = -2\pi i \sum_{v=1}^{\infty} \frac{\kappa_2^2 \{[(-1)^{m+n} + 1] e^{i\zeta|\gamma|} - (-1)^m e^{i\zeta|\gamma+2a|} - (-1)^n e^{i\zeta|\gamma-2a|}\}}{h\zeta(\zeta^2 - \alpha_m^2)(\zeta^2 - \alpha_n^2)\alpha^4} \Bigg|_{\zeta=\sqrt{k_2^2 - (v\pi/h)^2}}$$

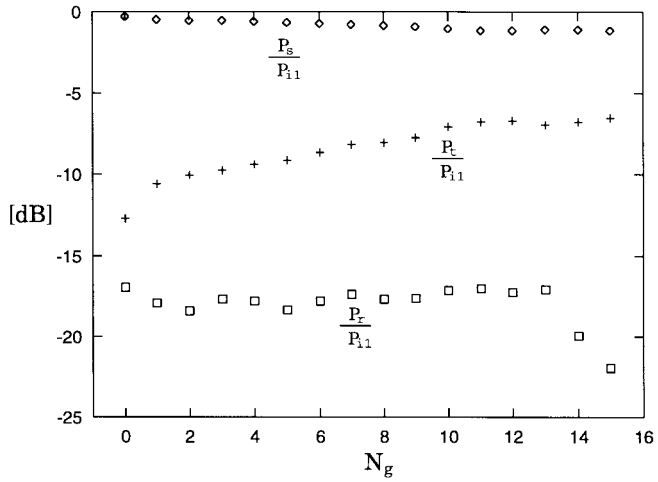

Fig. 3. Reflected, transmitted, and scattered powers versus N_g ($a_s = a_g = 0.167\lambda$, $T_s = T_g = 0.667\lambda$, $h = 0.6\lambda$, $d = 0.2\lambda$, $t = 0$, $x_d = 0.07\lambda$, $N_s = 12$, $\epsilon_{r1} = \epsilon_{r2} = 2.24$, $\epsilon_{r3} = \epsilon_{r4} = 1$).

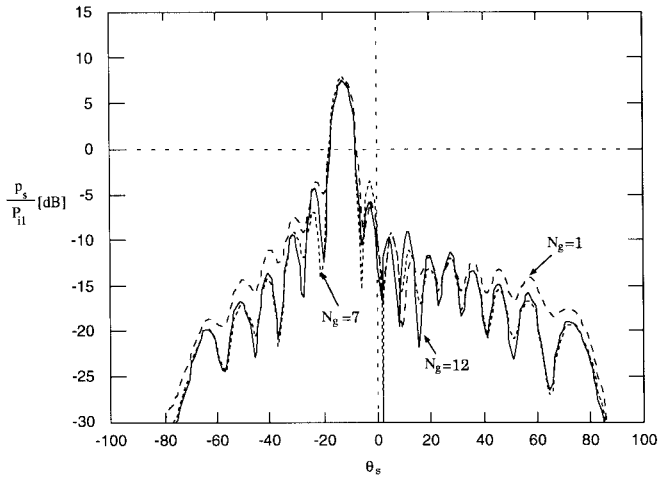

Fig. 4. Angular radiation pattern versus N_g ($a_s = a_g = 0.167\lambda$, $T_s = T_g = 0.667\lambda$, $h = 0.6\lambda$, $d = 0.2\lambda$, $t = 0$, $x_d = 0.07\lambda$, $N_s = 12$, $\epsilon_{r1} = \epsilon_{r2} = 2.24$, $\epsilon_{r3} = \epsilon_{r4} = 1$).

$$\alpha_2(\zeta) = \sum_{l=-L_1^g}^{L_2^g} \sum_{m=1}^{\infty} u_m^l a_{gm} a_g^2 \sin(\xi_m d) \times F_m(a_g\zeta) e^{i\zeta(x_d + tT_g)}. \tag{30}$$

When $A_1 = 1$ and $A_2 = 0$, the time-averaged incident, reflected, transmitted and radiated [scattered into Region (III)] powers are, respectively

$$P_{i1} = \frac{k_{xs} h}{4\omega\mu_0} \tag{31}$$

$$P_r = \frac{h}{4\omega\mu_0} \sum_v k_{xv}^* |K_v(k_{xv})|^2 \tag{32}$$

$$P_t = \frac{h}{4\omega\mu_0} \left[k_{xs}^* |1 + (-1)^s K_s(-k_{xs})|^2 + \sum_{v \neq s} k_{xv}^* |K_v(-k_{xv})|^2 \right] \tag{33}$$

$$P_s = \sum_{w=-L_1^s}^{L_2^s} \sum_{k=1}^{\infty} \frac{-a_s}{2\omega\mu_0} \times \mathrm{Re}\{i\chi_k^* [b_k^w \cos(\chi_k t) + c_k^w \sin(\chi_k t)] \times [b_k^w \sin(\chi_k t) - c_k^w \cos(\chi_k t)]^*\} \tag{34}$$

where the symbols $\mathrm{Re}(\cdots)$ and $(\cdots)^*$ denote a real part and a complex conjugate of $(\cdots)$. The power conservation requires $P_r + P_t + P_s = P_{i1}$.

When $A_1 = 0$ and $A_2 = 1$

$$P_{i2} = \frac{aN_s k_z}{\omega\mu_0} \tag{35}$$

$$P_r = \frac{h}{4\omega\mu_0} \sum_v k_{xv}^* |K_v(k_{xv})|^2 \tag{36}$$

$$P_t = \frac{h}{4\omega\mu_0} \sum_v k_{xv}^* |K_v(-k_{xv})|^2. \tag{37}$$

The far-zone scattered field at distance $x = r \sin\theta_s$ and $(z + h + t) = r\cos\theta_s$ is

$$E_y^s(r, \theta_s) = \sqrt{\frac{k_4}{2\pi r}} \cos\theta_s \tilde{E}_y^s(-k_4 \sin\theta_s) e^{i(k_4 r - \pi/4)}. \tag{38}$$

Therefore, the far-zone scattered power density $p_s(r, \theta_s)$ is

$$p_s(r, \theta_s) = \tfrac{1}{2}\mathrm{Re}[E_y^s(r, \theta_s) H_\theta^{s*}(r, \theta_s)] \tag{39}$$

$$P_s = \int_{-\pi/2}^{\pi/2} p_s(r, \theta_s) r\, d\theta_s \tag{40}$$

$$= \frac{k_4}{4\pi} \sqrt{\frac{\epsilon_4}{\mu_0}} \int_{-\pi/2}^{\pi/2} |\tilde{E}_y^s(-k_4 \sin\theta_s)|^2 \cos^2\theta_s\, d\theta_s. \tag{41}$$

In what follows, we evaluate the radiation from a slitted parallel-plate when $A_1 = 1$ and $A_2 = 0$. We also assume that $L_1^g = L_1^s = 0$. We investigate the effects of the grooves on the radiation and scattering in Fig. 3. Fig. 3 shows a variation of the scattered (P_s/P_{i1}), transmitted (P_t/P_{i1}), and reflected (P_r/P_{i1}) powers versus the number of the grooves N_g. The total radiation power seems to be less sensitive to a change in N_g, indicating that the effects of the grooves are not significant. This is because the groove size is small ($a_g < 0.5\lambda/\sqrt{\varepsilon_{r1}}$) so that the waves inside the grooves are all evanescent in the z direction. Fig. 4 shows the effects of N_g on the angular radiation pattern (rp_s/P_{i1}). Fig. 4 illustrates that an increase in the number of grooves (N_g) results in a slight decrease in both the sidelobe levels and the mainlobe beamwidth. This means that the mainlobe beamwidths (or sidelobe levels) with $N_g = 7$ and 12 are slightly narrower (or lower) than those with $N_g = 0$. We do not show the curve with $N_g = 0$ since it is almost the same as the one with $N_g = 1$. Fig. 5 shows the effects of x_d/λ (x_d: displacement of the centers of groove and slit) on the reflected, transmitted, and the total scattered powers. When x_d/λ is between 0.06–0.12, the total scattered power becomes maximum with P_r/P_{i1} and $P_t/P_{i1} \leq -10$ dB. Our computational experience indicates that all propagation modes associated with the grooves and

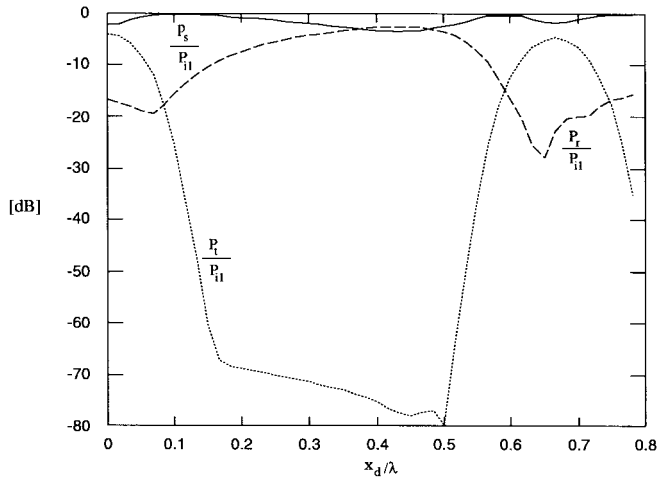

Fig. 5. Reflected, transmitted, and scattered powers versus x_d ($a_s = a_g = 0.167\lambda$, $T_s = T_g = 0.667\lambda$, $h = 0.6\lambda$, $d = 0.2\lambda$, $t = 0$, $N_s = N_g = 24$, $\epsilon_{r1} = \epsilon_{r2} = 2.24$, $\epsilon_{r3} = \epsilon_{r4} = 1$, (I): [5]).

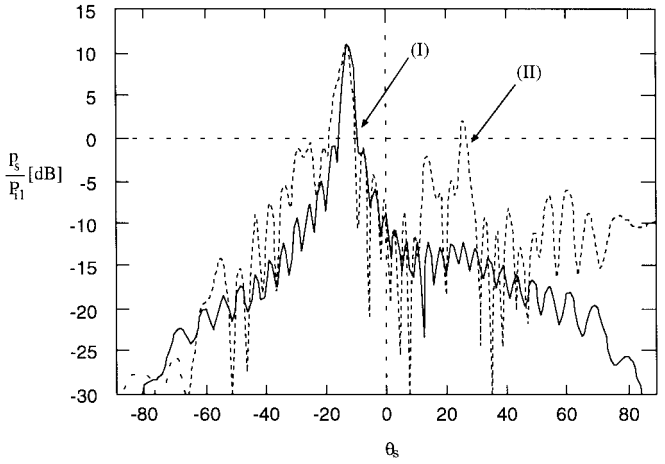

Fig. 6. Comparison of radiation pattern between theory (I) and measurement (II) ($a_s = a_g = 0.167\lambda$, $T_s = T_g = 0.667\lambda$, $h = 0.6\lambda$, $d = 0.2\lambda$, $t = 0$, $x_d = 0.07\lambda$, $N_s = N_g = 24$, $f = 12$ GHz, $w = 20$ cm, $\epsilon_{r1} = \epsilon_{r2} = 2.24$, $\epsilon_{r3} = \epsilon_{r4} = 1$).

slits must be considered in numerical computation in order to achieve the numerical accuracy within 1% error. Fig. 6 shows the comparison between the measurement and our theory in the angular radiation pattern (rp_s/P_{i1}) in the H plane. In the measurement, a hog-horn feed is used to excite the slitted parallel-plate antenna whose dimensions (length $\times$ width) are 400 cm $\times$ 20 cm in the x–y directions. A reasonable agreement in the mainlobe level is seen between the theory and the measurement while there is some discrepancy in the sidelove levels. The discrepancy in the sidelobes may be attributed to the effects of the reflection resulting from an abrupt termination of the antenna in the $+x$ direction. We also presume that a use of the finite line-current source realized by the hog-horn feed may be responsible for the discrepancy.

IV. Conclusion

The TE-wave radiation from a slitted parallel-plate with rectangular grooves is analyzed. The numerically efficient series solution is obtained to evaluate the radiation pattern and the reflection coefficient. The effects of the grooves on the radiation pattern are discussed. The measured angular pattern near the mainlobe agrees with the theoretical prediction.

Acknowledgment

The authors would like to thank the Division of Electromagnetic Metrology, Korea Research Institute of Standards and Science, Taejon, for the antenna pattern measurements.

References

[1] E. M. T. Jones and J. K. Shimizu, "A wide-band transverse-slot flush-mounted array," *IRE Trans. Antennas Propagat.*, pp. 401–407, July 1960.

[2] A. M. Barbosa, A. F. dos Santos, and J. Figanier, "Radiation field of a periodic strip grating excited by an aperiodic line source," *Radio Sci.*, vol. 19, no. 3, pp. 829–839, May/June 1984.

[3] C. W. Chuang, "Generalized admittance matrix for a slotted parallel-plate waveguide," *IEEE Trans. Antennas Propagat.*, vol. 36, pp. 1227–1230, Sept. 1988.

[4] J. A. Encinar, "Mode-matching and point-matching techniques applied to the analysis of metal-strip-loaded dielectric antennas," *IEEE Trans. Antennas Propagat.*, vol. 38, pp. 1405–1412, Sept. 1990.

[5] J. H. Lee, H. J. Eom, and J. W. Lee, "Scattering and radiation from finite thick slits in parallel-plate waveguide," *IEEE Trans. Antennas Propagat.*, vol. 44, pp. 212–216, Feb. 1996.

[6] J. H. Lee, H. J. Eom, J. W. Lee, and K. Yoshitomi, "Transverse electric mode scattering from rectangular grooves in parallel-plate," *Radio Sci.*, vol. 29, no. 5, pp. 1215–1218, Sept./Oct. 1994.

Jung Hyeong Lee was born in Korea on March 28, 1968. He received the B.S., M.S., and Ph.D. degrees in electrical engineering from Korea Advanced Institute of Science and Technology (KAIST), Taejon, Korea, in 1992, 1994, and 1997, respectively.

In 1997, he joined the telecommunication network systems division of information and communication business of SamSung Electronics Co., Ltd, where he is Senior Engineer of high-speed transmission group of access network team. He is researching the digital microwave radio system transmitting STM-1 (155.520 Mbps). His research interests are in mobile communication, digital signal processing, and communication networks.

Hyo Joon Eom (S'78–M'82) received the B.S. degree in electronic engineering from Seoul National University, Korea, and the M.S. and Ph.D. degrees in electrical engineering from the University of Kansas, Lawrence, KS, in 1977 and 1982, respectively.

From 1981 to 1984, he was a Research Associate at the Remote Sensing Laboratory, University of Kansas. From 1984 to 1989 he was with the faculty of the Department of Electrical Engineering and Computer Science, University of Illinois, Chicago, IL. In 1989 he joined the Department of Electrical Engineering, Korea Advanced Institute of Science and Technology, where he is currently a Professor. His research interests are wave scattering and antenna.